Molecules and Cells

Small Molecule-Based Strategy Promotes Nucleus Pulposus Specific Differentiation of Adipose-Derived Mesenchymal Stem Cells

Jianming Hua[1,5], Ning Shen[2,5], Jingkai Wang[3,4,5], Yiqing Tao[3,4], Fangcai Li[3,4], Qixin Chen[3,4,*], and Xiaopeng Zhou[3,4,*]

[1]Department of Radiology, 2nd Affiliated Hospital, School of Medicine, Zhejiang University, Hangzhou 310009, China, [2]Department of Rheumatology, Sir Run Run Shaw Hospital, School of Medicine, Zhejiang University, Hangzhou 310016, China, [3]Department of Orthopedics Surgery, 2nd Affiliated Hospital, School of Medicine, Zhejiang University, Hangzhou 310009, China, [4]Orthopedics Research Institute of Zhejiang University, Hangzhou 310009, China, [5]These authors contributed equally to this work.
*Correspondence: doctorzxp@zju.edu.cn (XZ); zrcqx@zju.edu.cn (QC)
https://doi.org/10.14348/molcells.2019.0098
www.molcells.org

Adipose tissue-derived mesenchymal stem cells (ADSCs) are promising for regenerating degenerated intervertebral discs (IVDs), but the low efficiency of nucleus pulposus (NP)-specific differentiation limits their clinical applications. The Sonic hedgehog (Shh) signaling pathway is important in NP-specific differentiation of ADSCs, and Smoothened Agonist (SAG) is a highly specific and effective agonist of Shh signaling. In this study, we proposed a new differentiation strategy with the use of the small molecule SAG. The NP-specific differentiation and extracellular matrix (ECM) synthesis of ADSCs were measured *in vitro*, and the regenerative effects of SAG pretreated ADSCs in degenerated IVDs were verified *in vivo*. The results showed that the combination of SAG and transforming growth factor-β3 (TGF-β3) is able to increase the ECM synthesis of ADSCs. In addition, the gene and protein expression levels of NP-specific markers were increased by treatment with SAG and TGF-β3. Furthermore, SAG pretreated ADSCs can also improve the disc height, water content, ECM content, and structure of degenerated IVDs *in vivo*. Our new differentiation scheme has high efficiency in inducing NP-specific differentiation of ADSCs and is promising for stem cell-based treatment of degenerated IVDs.

Keywords: adipose-derived mesenchymal stem cell, differentiation, nucleus pulposus, Smoothened Agonist, transforming growth factor-β3

INTRODUCTION

Intervertebral disc (IVD) degeneration and the consequent low back pain affect approximately 80% of people in Western countries and is the leading cause of disability especially in people aged less than 45 years (Andersson, 1999; Sakai and Andersson, 2015; Vos et al., 2012). The IVD is composed of a central nucleus pulposus (NP) and surrounded by the annulus fibrosus (AF) and thin hyaline cartilaginous endplates (Eyring, 1969). NP degeneration caused by the dysfunction of NP cells and disappearance of extracellular matrix (ECM) is thought to initiate IVD degeneration (Chen et al., 2006).

There is no ideal treatment for IVD degeneration now since conservative or surgical therapies do not restore IVD tissue properties. Stem cell-based therapy exhibits novel promise for regenerating degenerated IVDs (Wang et al., 2014). Mesenchymal stem cells (MSCs) are currently the most widely

Received 19 May, 2019; revised 6 August, 2019; accepted 21 August, 2019; published online 23 September, 2019

eISSN: 0219-1032

used graft cell for IVD regeneration due to their self-renewal capability and multilineage differentiation potential (Jia et al., 2018; Tam et al., 2014; Vaudreuil et al., 2018). Adipose tissue-derived mesenchymal stem cells (ADSCs) can be obtained more easily than NP-derived MSCs and have the potential to differentiate towards an NP-like phenotype under specific conditions (Richardson et al., 2016; Zhu et al., 2017). Transforming growth factor (TGF)-β3 is widely used to induce the NP-like differentiation of MSCs (Gan et al., 2016; Tsaryk et al., 2015). However, TGF-β3 also induces chondrogenic differentiation of ADSCs, and the efficiency of NP-specific differentiation cannot meet clinical treatment needs (Huang et al., 2018; Qu et al., 2019). New methods should be carried out to improve the efficiency of NP-specific differentiation of ADSCs.

The Sonic hedgehog (Shh) signaling pathway is important for notochord development, and the inhibition of the Shh signaling pathway in the embryos results in vertebral column patterning defects (Choi et al., 2012). Shh signaling is also required for the postnatal growth and differentiation of IVDs (Dahia et al., 2012). Studies have demonstrated that activation of the Shh signaling pathway leads to the generation of healthy NP cells (Choi et al., 2008). The Shh signaling pathway is also important in regulating stem cell proliferation and differentiation (Komada, 2012; Vazin et al., 2014). Activation of the Shh signaling pathway can contribute to the synthesis of proteoglycans and type II collagen in MSCs (Chen et al., 2019). In our previous studies, Gli1-dependent Shh signaling was activated during the NP-like differentiation of ADSCs (Zhou et al., 2018a). Therefore, the Shh signaling pathway is a key regulator of NP-like differentiation, and activation of the Shh signaling pathway may improve the efficiency of NP-specific differentiation of ADSCs.

The Shh signaling pathway mainly comprises Patched (Ptch), Smoothened (Smo), Costal2, Fused (FU), suppressor of FU (SUFU), and Gli transcription factors. In the absence of Shh, the membrane guanosine triphosphate-binding protein coupled receptor-like protein Smo is tonically inhibited by Ptch. After Shh binds to Ptch on the plasma membrane, Smo is activated and recruits a downstream protein complex including Costal2, FU and SUFU. Then, Gli transcription factors such as Gli1 and Gli2 are activated and induce target genes (Briscoe and Small, 2015; Yao et al., 2016). Small molecules are widely used to regulate the activity of signaling pathways. In the Shh signaling pathway, Smo is directly activated by the small molecule agonist Smoothened Agonist (SAG) and then activates Shh signaling (Chen et al., 2002; Stanton and Peng, 2010). SAG is a highly specific and effective Smo agonist and can produce results generally superior to conventional protein reagents (Lewis and Krieg, 2014). Wang et al. (2013) activated Shh signaling in hepatocellular carcinoma cells by SAG. Seifert et al. (2012) demonstrated that SAG can activate Gli1 and induce the expression of growth factors in fibroblasts. However, the effects of SAG in inducing NP-specific differentiation of ADSCs have not yet been clarified.

We designed this study to clarify the effects of the small molecule SAG on the NP-specific differentiation of ADSCs. We further sought to determine the regenerative effects of SAG-induced ADSCs on degenerated IVDs *in vivo*. Use of the small molecule SAG may provide a new approach for NP-specific differentiation of ADSCs and promote the application of stem cell-based therapy in IVDs.

MATERIALS AND METHODS

Culture of stem cells

Human adult ADSCs of passage 2 were bought from Cyagen Biosciences (China). Human ADSCs basal culture medium (Cyagen Biosciences) supplemented 10% fetal bovine serum, 1% penicillin-streptomycin and 1% glutamine was used to culture the stem cells, and changed every three days. The stem cells were cultured in a humidified incubator at 37°C with 5% CO_2, and cells of passages 4 to 6 were used in subsequent experiments.

Cell differentiation

ADSCs were cultured on 12-well plates coated with Matrigel (BD Biosciences, China) and added with normal (Dulbecco's modified Eagle's medium [DMEM]/high glucose supplemented with 1% fetal bovine serum, 1% ITS+3, 50 nM ascorbate-2-phospate, 40 ng/ml dexamethasone, and 1% penicillin-streptomycin solution) or differentiation medium (normal medium supplemented with 10 ng/ml TGF-β3). Different concentrations (0, 0.1, 0.5, and 2.5 μM) of SAG (Selleckchem, USA) was added to induce NP-specific differentiation of ADSCs. All groups were incubated at 37°C with 5% CO_2 and the culture medium was changed every three days.

Alcian blue staining

After 21 days of cultivation, all groups were washed three times with phosphate buffered saline (PBS) and fixed using 4% paraformaldehyde for 15 min. The cells were then stained with Alcian blue solution for 30 min at room temperature, followed by washing with PBS. Alcian blue staining were observed and images were collected with a microscope (Leica, Germany).

Gene expression analysis

RNAiso reagent (TAKARA, China) was used to extract total RNA, and PrimeScriptTM RT Reagent Kit (TAKARA) was used to perform the reverse transcription. mRNA was quantified by quantitative polymerase chain reaction (qPCR) using SYBR Green (TAKARA) on the StepOnePlus Real-time PCR System (Applied Biosystems, USA). 18s rRNA was used as housekeeping gene, and the expression of each target gene was normalized to the expression of 18s rRNA (Table 1). All primers were synthesized by Sangon Biotech (China). Gene expression was calculated by the $2^{-\Delta\Delta Ct}$ method.

Protein expression analysis

Total protein of each group was extracted by RIPA buffer containing 1% phenylmethanesulfonyl fluoride, and the concentrations were measured with a BCA quantification kit (Pierce, China). Proteins were separated by sodium dodecyl sulfate polyacrylamide gel electrophoresis and transferred onto polyvinylidene fluoride membranes (Millipore, USA). The membranes were blocked with 5% skim milk in Tris-buffered saline with 0.1% Tween-20 (TBST) at room temperature for

Table 1. Primers used in quantitative RT-PCR

Gene	Forward primer (5' to 3')	Reverse primer (5' to 3')
18s	GAATTCCCAGTAAGTGCGGGTCATA	CGAGGGCCTCACTAAACCATC
Acan	CTAGCTGCTTAGCAGGGATAACG	GATGACCCGCAGAGTCACAAAG
Sox9	AGGAAGCTGGCAGACCAGTACC	GGGTCTCTTCTCGCTCTCGTTCA
Col2a1	CTGGTGGAGCAGCAAGAGC	GTGGACAGTAGACGGAGGAAAG
Col1a1	ACCTCCGGCTCCTGCTCCTCTTA	GACAGCACTCGCCCTCCCGTTTTT
Krt19	CCGACCTGGAGATGCAGATAGAG	TAGGTCAATGCCTGGTGTGGAA
Pax1	CTCCTTAGGGCCACCGCT	TTAATTGACGTTCCGATCCTGC
Gdf10	ACAGTGTGCAGAGGGACAGG	CTTCTGGTCGATCACATCCAGC
Cd24	CCGAGCATCCAGAGAGTCG	GCAATAAATCTGCGTGGGTAGG
Shh	CTATGAGGGTCGAGCAGTGG	CGGAGTTCTCTGCTTTCACAG
Gli1	CTATGGTGAGCCATGCTGTC	GAAAGTCCTTCTGTTCCCATGC
Gli2	CCCCTACCGATTGACATGCG	GAAAGCCGGATCAAGGAGATG
Ptch1	GGACTTACGTGGAGGTGGTT	TGGTTAAACAGGCGTAGGCA

1 h, followed by incubating with appropriate primary antibodies overnight at 4°C in TBST: SOX9 (1:1,000; Abcam, UK), aggrecan (1:1,000; Abcam), collagen II (1:5,000; Abcam), KRT19 (1:1,000; Abcam), PAX1 (1:400; Abcam), GDF10 (1:400; Abcam), Shh (1:1,000; Cell Signaling Technology, China), PTCH1 (1:1,000; Cell Signaling Technology), Gli1 (1:1,000; Abcam), Gli2 (1:500; Abcam), Smad3 (1:1,000; Cell Signaling Technology), p-Smad3 (1:1,000; Cell Signaling Technology), or GAPDH (1:5,000; Santa Cruz, China). After that, the membranes were incubated with horseradish peroxidase-labeled secondary antibodies (1:5,000; Santa Cruz) at room temperature for 1 h, and immunoreactivity was detected using an enhanced chemiluminescence substrate (Millipore, China). The relative protein levels were quantified by densitometry using the Quantity One Software (Bio-Rad Laboratories, Germany).

Enzyme-linked immunosorbent assay (ELISA)

The concentration of Shh protein in each medium was determined using a Shh ELISA kit (R&D Systems, China) according to the manufacturer's protocols. A standard curve was calculated using known concentrations of Shh protein. Absorbance values at 450 nm were measured using a Model 680 microplate reader (Bio-Rad Laboratories).

Immunofluorescence staining

Cells were washed three times with PBS and fixed using 4% paraformaldehyde for 15 min. After that, cells were permeabilized with 0.05% Triton X-100 for 15 min and blocked with 5% bovine serum albumin (BSA) for 1 h at room temperature. Cells were then incubated with collagen II (1:200; Abcam) in 1% BSA overnight at 4°C. Alexa Fluor 555-labeled secondary antibody (Beyotime, China; excitation and emission wavelengths are 555 and 565 nm) was used to incubate cells at room temperature for 1 h. Nuclei were then stained with 4',6-diamidino-2-phenylindole (DAPI; Sigma Aldrich, China) at room temperature for 10 min. Immunofluorescence were observed and images were collected using a fluorescence microscope (DM5500; Leica).

Animal and surgical procedure

Rat tail disc degeneration model was used in the *in vivo* experiments. Sixteen males Sprague-Dawley rats weighting 200 g were obtained from the Animal Center of the Academy of Medical Science of Zhejiang Province. All procedures were approved by the Institutional Animal Care and Use Committee of Zhejiang University and the surgical procedures had already been reported in our previous study (Zhou et al., 2018b). Briefly, anesthesia was performed by intraperitoneal injection with 1% pentobarbital sodium, and a 20-G sterile needle was inserted into the disc of coccygeal vertebrae (Co)7/Co8 and Co8/Co9 at a depth from skin to the middle of the disc. After that, the needle was rotated 360° and held for 30 s. ADSCs were pre-cultured in differentiation medium with or without 0.5 μM SAG for 14 days. Two weeks after the surgical procedure, the SD rats were randomized into four groups: the control group (without needle puncture and other treatments); the degeneration group (with needle puncture and DMEM injection); the ADSC group (with needle puncture and ADSCs injection); the SAG-ADSC group (with needle puncture and SAG treated ADSCs injection). A microsyringe attached to a 31-G needle was used to deliver 2 μl of materials to the NP.

Radiographic measurement and magnetic resonance imaging (MRI) evaluation

The rats were anesthetized and placed in the prone position and kept their tails straight. Radiographs of the rat tails were taken using a molybdenum target radiographic image unit (GE Mammography DMR Bucky 18 × 24; GE Healthcare, UK) at 16 weeks after injection. Disc height index (DHI%) analyzed qualitatively from digitized radiographs was used to quantitatively describe disc height changes. The T2-weighted midsagittal sections of rat tails were obtained by a 3.0 T MRI scanner (GE Medical Systems, UK) at 16 weeks after injection. The parameter settings were as follows: spin echo repetition time, 3,500 ms; echo time, 100 ms; field of view, 12 × 9 cm; slice thickness, 3 mm. MRI index (the area of the NP multiplied by average signal intensity) were analyzed qualitatively using a GE ADW4.2 workstation for evidence of water content and degenerative changes. Two researchers conducted all these

assessments independently in a blinded fashion.

Histological and biochemical analysis

Samples of rat tails were harvested at 16 weeks after injection. Samples were rinsed with PBS, fixed in 4% paraformaldehyde for 72 h, and decalcified using 10% EDTA (Sigma Aldrich) for 30 day at room temperature. After that, samples were embedded in paraffin, and cross-sectioned (3 μm). Safranine O-fast green, and H&E were performed separately on consecutive tissue sections. Images were obtained using a microscope (BX51; Olympus, Japan).

For biochemical analysis, NP samples of rats were frozen at −80°C and lyophilized for 24 h, and the weight of samples were measured and recorded as dry weight. After that, samples were digested with 125 μg/ml papain (Sigma) for 18 h at 60°C. The contents of sulfated glycosaminoglycans (sGAG) and hydroxyproline of each group were detected using the Blyscan assay (Biocolor, China) and Hydroxyproline Assay Kit (Jiancheng Bioengineering Institute, China), respectively, and the experimental procedures were carried out following the manufacturer's protocols. The contents of sGAG and hydroxyproline were normalized with sample dry weight.

Statistical analysis

The data was analyzed with IBM SPSS Statistics (ver. 22.0 for Windows; IBM, USA). Statistical significance of the differences between experimental groups was assessed using a two-tailed Student's *t*-test for comparisons of two groups and one-way analysis of variance following Tukey's post hoc test for multiple pairwise comparisons. A value of $P < 0.05$ was considered to indicate statistical significance. The results were expressed as the mean ± SEM. All experiments were repeated at least in triplicate using independent samples.

RESULTS

SAG increased the ECM synthesis of ADSCs

The expression levels of ECM synthesis related genes such as *Acan*, *Sox9*, *Col2*, and *Col1* were measured by qPCR on day 14. As the concentration of SAG increased, the gene expression of *Acan* increased gradually. However, there was no significant difference between the 0.5 and 2.5 groups. The gene expression of Sox9 in the 0.5 group showed no significant difference from that of the 2.5 group but was significantly higher than that in the other two groups. The expression of *Col2* in the 0.5 group was almost 13.75- and 6.11-fold higher than that of the 0 and 0.1 groups. No significant difference in *Col1* expression was observed between each concentration gradient (Fig. 1A). The protein expression of aggrecan, SOX9, and COL2 was detected using western blotting on day 21. As the concentration of SAG increased from 0 to 0.5 μM, the expression of aggrecan increased gradually. Higher expression of SOX9 was observed with SAG concentrations of 0.5 and 2.5 μM than with the 0 and 0.1 μM concentrations. The protein expression levels of COL2 in the 0.1, 0.5, and 2.5 groups were similar but were all higher than that of the 0 group (Fig. 1B). The sGAG synthesis of ADSCs was shown by Alcian blue staining on day 21. When the concentrations of SAG were 0.5 and 2.5 μM, the sGAG, which were stained blue, could be observed clearly. The staining in the 0.5 and 2.5 groups was deeper than that in the 0 and 0.1 groups (Fig. 1C).

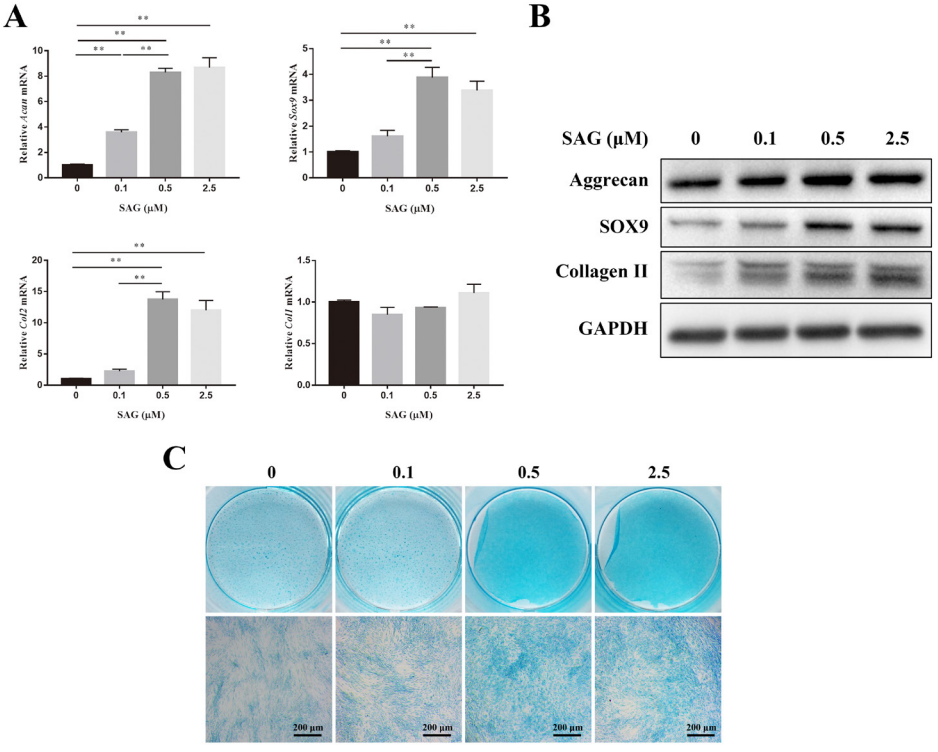

Fig. 1. SAG increased the ECM synthesis of ADSCs. (A) Gene expression levels of *Acan*, *Sox9*, *Col2*, and *Col1* of ADSCs cultured in differentiation medium with different concentrations of SAG were measured on day 14 and normalized to 18s and to the control group. Data represent mean ± SEM. $^{**}P < 0.01$. (B) The protein expression of aggrecan, SOX9 and collagen II of ADSCs were measured by western blotting analysis on day 21. (C) sGAG synthesized by ADSCs was observed by Alcian blue staining on day 21. Scale bars = 200 μm.

SAG induced the NP-specific differentiation of ADSCs

The NP-specific differentiation of ADSCs was determined by qPCR and western blotting. KRT19, PAX1, and CD24 are specific markers of NP cells, while GDF10 is a specific marker of chondrocytes (Lee et al., 2007; Minogue et al., 2010). Differentiation medium supplemented with 0 or 0.5 μM SAG was used to induce the differentiation of ADSCs. The gene expression of *Krt19* was significantly increased after the addition of SAG on days 14 and 21. The gene expression of *Pax1* in ADSCs was also increased after the induction of SAG, but no significant difference was observed. SAG (0.5 μM) significantly increased the gene expression of *Cd24* in ADSCs on days 14 and 21. The 0.5 μM group showed significantly lower gene expression of Gdf10 than the 0 μM group on days 14 and 21 (Fig. 2A). After 14 and 21 days of cultivation, the protein expression of KRT19 in the 0.5 μM group was significantly increased compared with that in the 0 μM group. Both groups showed similar protein expression of PAX1 on days 7 and 14. However, SAG significantly increased the expression of PAX1 on day 21. The protein expression of GDF10 was significantly decreased after the addition of SAG on days 14 and 21 (Fig. 2B).

The Shh signaling pathway was activated by SAG and TGF-β3

Normal and differentiation medium was used to investigate the effects of TGF-β3 on the activation of the Shh signaling pathway in ADSCs. Both qPCR and western blotting were performed on day 14. SAG (0.5 μM) did not increase *Shh* gene expression in either normal or differentiation medium. However, TGF-β3 increased the gene expression of *Shh* with or without the addition of SAG (Fig. 3A). SAG increased the gene expression of *Ptch1*, *Gli1,* and *Gli2* in normal medium and significantly increased the expression of these three gene markers in differentiation medium. Compared with the normal medium, the differentiation medium also increased the

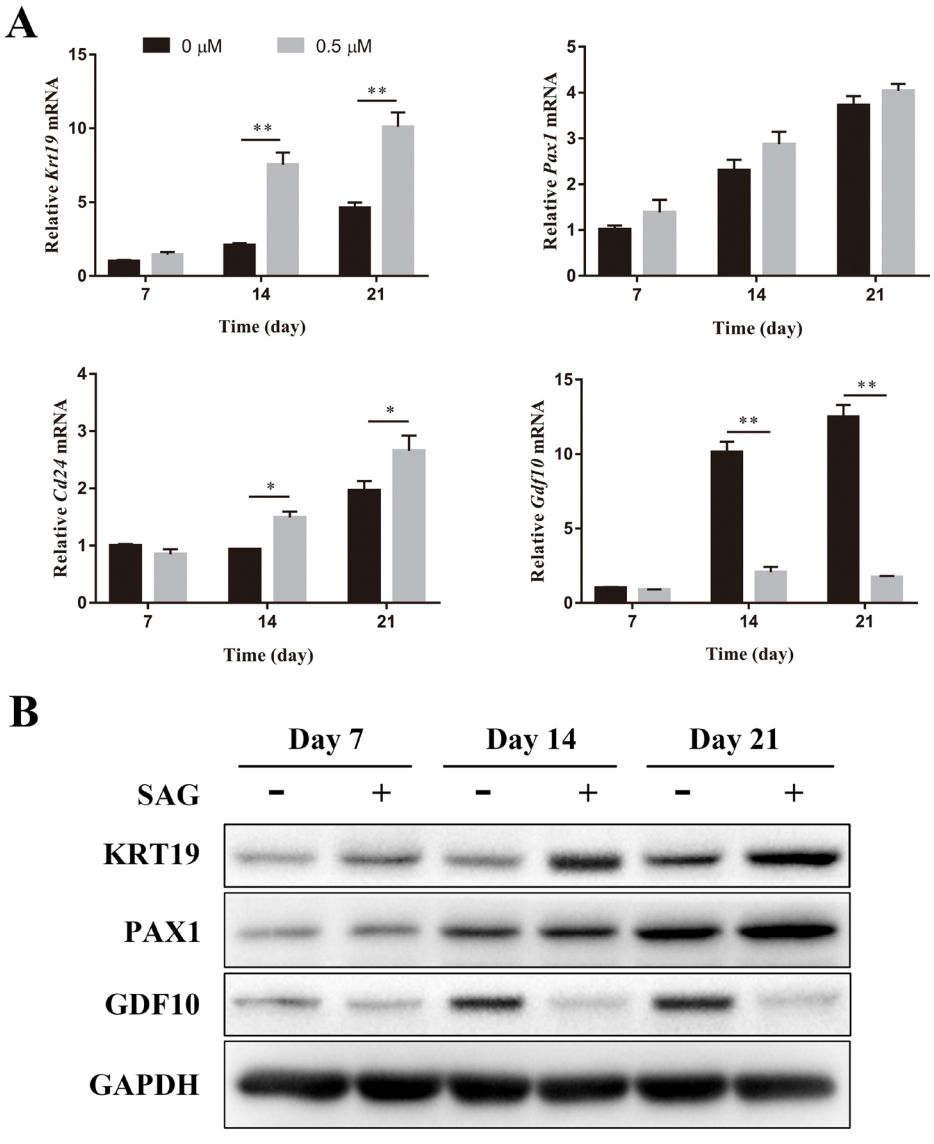

Fig. 2. SAG induced the NP-specific differentiation of ADSCs. (A) The gene expression level of *Krt19*, *Pax1*, *Cd24*, and *Gdf10* of ADSCs culture in differentiation medium with or without SAG was measured on days 7, 14, and 21 by PCR and normalized to 18s. Data represent mean ± SEM. $*P < 0.05$, $**P < 0.01$. (B) The protein expression of KRT19, PAX1, and GDF10 of ADSCs were determined by western blotting analysis on days 7, 14, and 21.

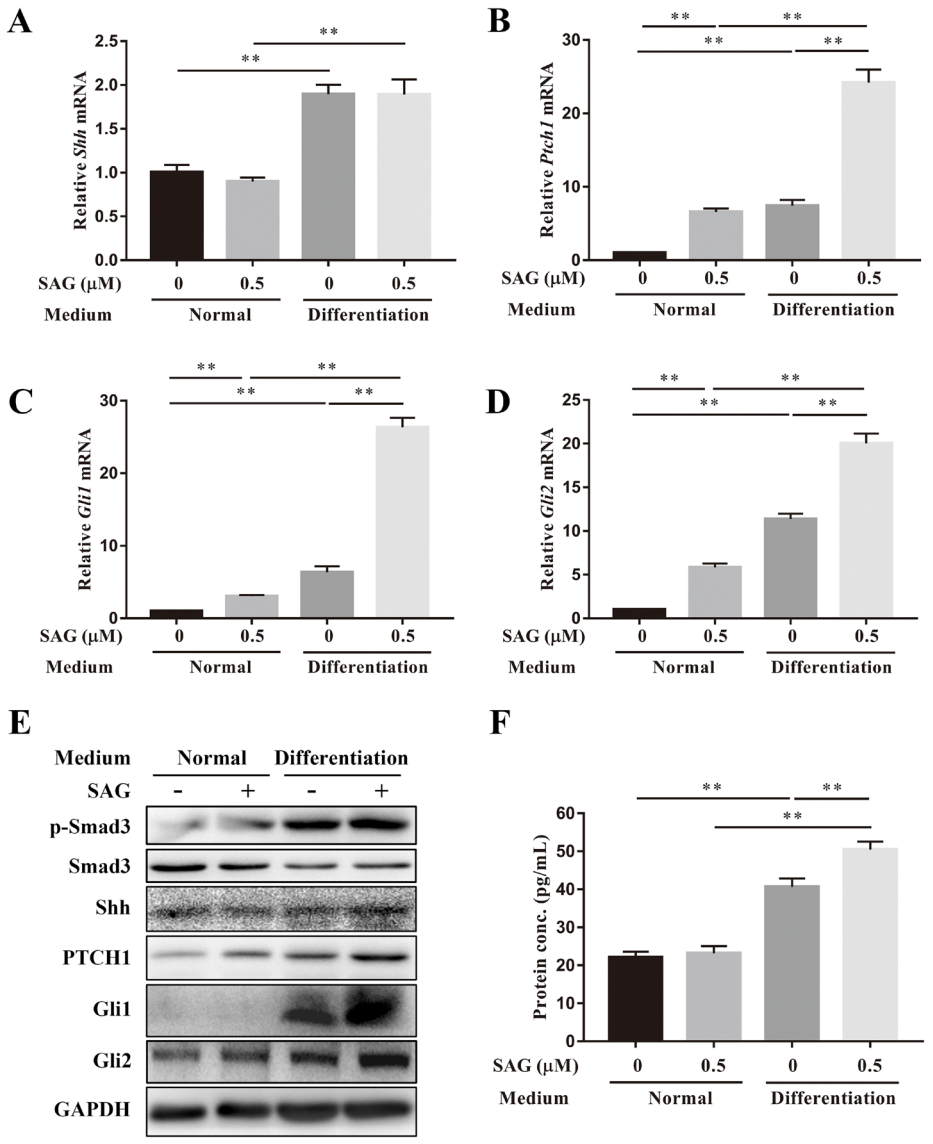

Fig. 3. The Shh signaling pathway was activated by SAG and TGF-β3. Gene expression levels of (A) *Shh*, (B) *Ptch1*, (C) *Gli1*, and (D) *Gli2* of ADSCs cultured in normal or differentiation medium with or without SAG were measured on day 14, and normalized to 18s. (E) The protein expression levels of p-Smad3, Smad3, Shh, PTCH1, Gli1, and Gli2 of ADSCs cultured in normal or differentiation medium with or without SAG on day 14 were measured. (F) The Shh protein secreted in medium during culture was quantified by ELISA. Data represent mean ± SEM. $^{**}P < 0.01$.

mRNA levels of *Ptch1*, *Gli1*, and *Gli2* with or without the addition of SAG (Figs. 3B and 3D). Phosphorylation of Smad3 was increased after TGF-β3 was added, and SAG did not affect the phosphorylation of Smad3 in either culture medium. There was no significant difference in the protein expression of Shh in the four groups. However, the results of ELISA showed the Shh protein secreted in differentiation medium was significantly higher than that in normal medium. The addition of SAG also increased the secretion of Shh protein in differentiation medium. TGF-β3 increased the protein expression of PTCH1, Gli1 and Gli2 with or without the addition of SAG. SAG increased the protein expression of PTCH1 but not Gli1 or Gli2 in normal medium. However, the protein expression of PTCH1, Gli1 and Gli2 was increased after SAG was added when ADSCs were cultured in differentiation medium (Figs. 3E and 3F).

Activation of the TGF-β signaling pathway promoted the activation of Shh signaling during the NP-specific differentiation of ADSCs

SB431542 is a selective inhibitor of TGF-β receptor I. After the addition of SB431542, the gene expression of *Gli1*, *Gli2*, *Ptch1*, *Krt19*, *Gdf10*, and *Col2* increased by SAG was partly rescued. SB431542 also significantly decreased the gene expression of *Ptch1* and *Gdf10* in ADSCs when SAG was absent (Fig. 4A). The phosphorylation of Smad3 was significantly inhibited by SB431542. Although the protein expression of Shh was not significantly affected by SB431542, the protein expression of PTCH1 was inhibited by SB431542, regardless of whether SAG was added. The protein expression of Gli1 and Gli2 increased by SAG was blocked by the inhibitor. These results indicated that the activation of Shh signaling is dependent on the TGF-β signaling pathway. The expression levels of KRT19, aggrecan, and COL2 were all increased by the induction of SAG but decreased after the addition of

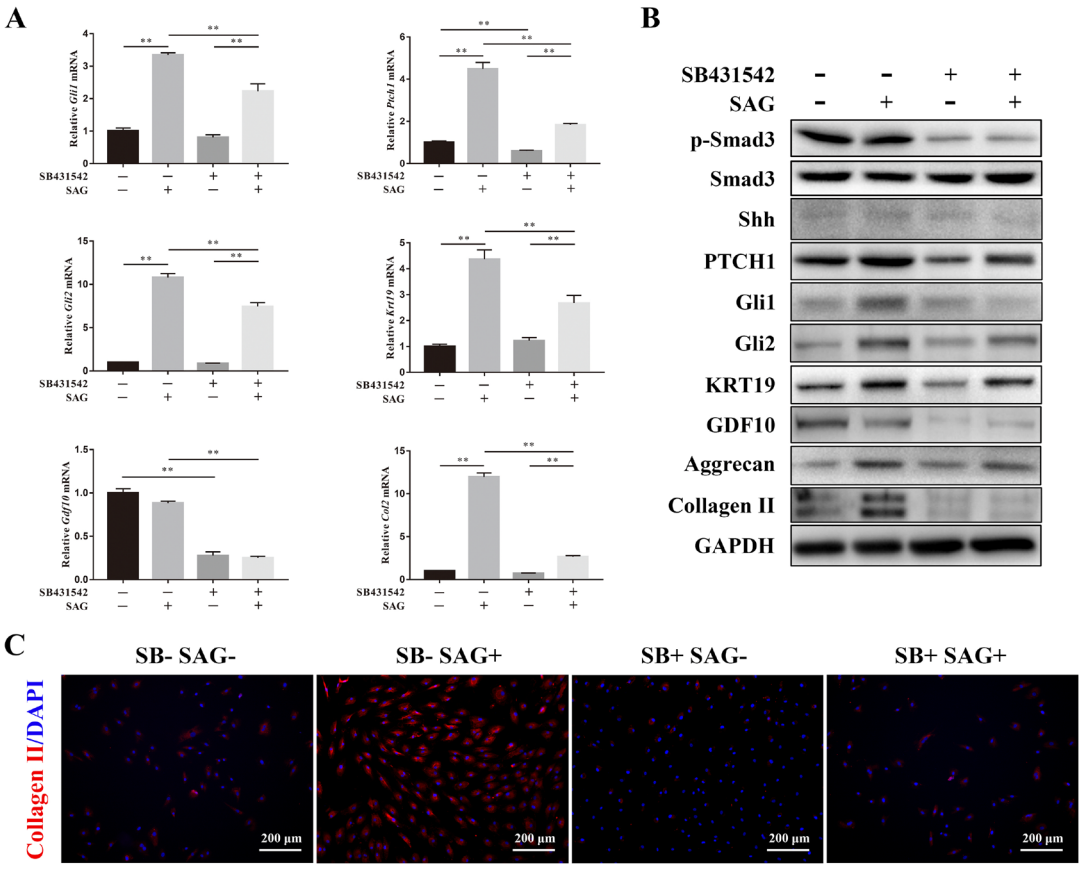

Fig. 4. Activation of the TGF-β signaling pathway promoted the activation of Shh signaling during the NP-specific differentiation of ADSCs. (A) SB431542 was used as an inhibitor of TGF-β receptor I. The gene expression level of *Gli1*, *Ptch1*, *Gli2*, *Krt19*, *Gdf10*, and *Col2* of ADSCs culture in differentiation medium were measured by PCR and normalized to 18s. Data represent mean ± SEM. $^{**}P < 0.01$. (B) The protein expression levels of p-Smad3, Smad3, Shh, PTCH1, Gli1, Gli2, KRT19, GDF10, aggrecan, Collagen II of ADSCs cultured in differentiation medium were measured by western blotting analysis. (C) Immunofluorescence staining showed the expression of collagen II (red) of cells, and the nuclei (blue) were stained with DAPI. Scale bars = 200 μm.

SB431542, which meant that the NP-specific differentiation and ECM synthesis of ADSCs could be improved by the simultaneous activation of Shh signaling and TGF-β signaling. Both SAG and SB431542 decreased the expression levels of GDF10, which meant the chondrogenic differentiation of ADSCs was blocked by Shh signaling and positively regulated by TGF-β signaling (Fig. 4B). We also detected the synthesis of collagen II by immunofluorescence staining and found that SAG significantly increased the synthesis of collagen II in ADSCs. However, the collagen II synthesis was significantly decreased after the addition of SB431542. No significant difference was observed between the SB-SAG- and SB+SAG+ groups (Fig. 4C).

SAG-treated ADSCs promoted the regeneration of degenerated IVD

After 16 weeks, the degeneration and ADSC groups showed significantly lower disc heights than the control group. No significant difference was observed between the control and SAG-ADSC groups in radiographic images (Fig. 5A). The DHI in the SAG-ADSC group was significantly higher than those in the degeneration and ADSC groups (Fig. 5B). The MRI results revealed the water content in each group. Compared with the control group, the other groups showed a lower T2 signal and MRI index. The T2 signal in the SAG-ADSC group was superior to that in the degeneration and ADSC groups. A significantly higher MRI index was observed in the SAG-ADSC group (2992.94 ± 107.42) than in the degeneration (1198.82 ± 70.11) and ADSC (1904.08 ± 147.31) groups (Figs. 5C and 5D).

H&E staining showed that the lamellar sheets of the AF in normal IVDs were regular and that the NP was well organized with cells and ECM. The structure of the AF and NP in the degenerated IVDs were destroyed. Fibrous connective tissues could be observed in the degeneration and ADSC groups. The NP in the SAG-ADSC group was more regular and well organized than that in the ADSC and degeneration groups. Safranin O staining indicated the proteoglycans in the IVD. Stronger staining in the SAG-ADSC group than in the degeneration and ADSC groups could be clearly observed. In addition, the Safranin O staining in the control group was stronger than that in the other groups (Fig. 6A). The contents of sGAG and

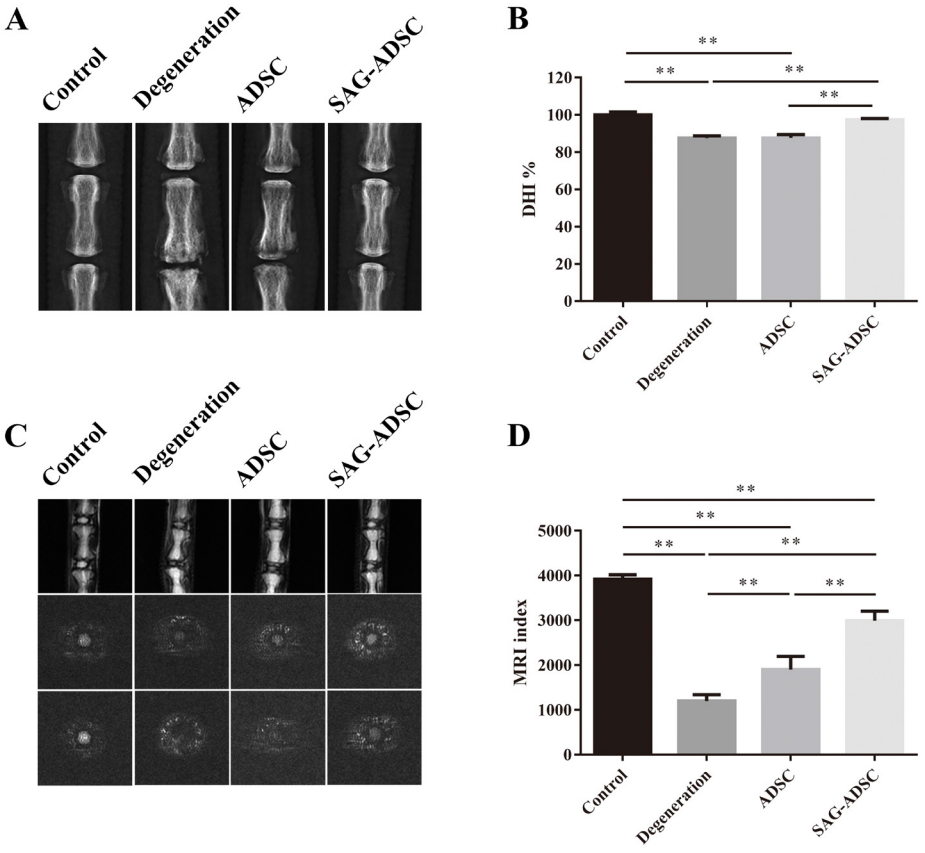

Fig. 5. Radiographic measurement and MRI evaluation of IVDs. (A) Representative radiographs of the rat Co7/Co8 and Co8/Co9 at 16 weeks after injection. The control, degeneration, ADSCs and SAG-ADSC groups were detected. (B) DHI% was used to quantitatively represent the disc height changes. (C) Representative T2 MRI scans of each group at 16 weeks after injection. (D) MRI index was used to quantitatively analyze the water content and structure of the NP. Data represent mean ± SEM. $^{**}P < 0.01$.

hydroxyproline were measured at week 16 and normalized to the NP dry weight. The contents of sGAG and hydroxyproline were significantly higher in the control group than in the other groups. The degeneration group had the lowest contents of sGAG and hydroxyproline of all groups. Moreover, the SAG-ADSC group exhibited a significant increase in sGAG and hydroxyproline contents compared with those in the degeneration and ADSC groups (Figs. 6B and 6C).

Histological scoring was used to evaluate the degeneration of IVD. The control group had a well-organized NP and AF, and the cellularity of the AF and NP were normal. The histological score of the control group was 5.40 ± 0.24. The morphology and cellularity of the NP and AF in the degeneration group was abnormal, and therefore the histological score of the degeneration group was 13.60 ± 0.60, which was significantly higher than that in the control group. The histological score of the SAG-ADSC group was 6.60 ± 0.24, which was significantly lower than that of the ADSC (8.60 ± 0.51) and degeneration groups. Although the SAG-ADSC group had a higher histological score than the control group, no significant difference was observed (Fig. 6D). The results indicated that SAG pretreated ADSCs could regenerate the degenerated IVD to some extent.

DISCUSSION

NP degeneration is thought to be the trigger of IVD degeneration. Directing the differentiation of ADSCs towards an NP-specific phenotype enables regenerating the degenerated NP (Fontana et al., 2014). However, the NP-specific differentiation of ADSCs is difficult to control, and the corresponding differentiation efficiency is low. A small molecular-based differentiation scheme is widely used to induce the specific differentiation of stem cells. Amirpour et al. (2019) induced the eye field neuroectoderm differentiation of ADSCs by three small molecules. Small molecular kartogenin has the ability to induce the chondrogenic differentiation of MSCs (Jing et al., 2019; Yang et al., 2019). Small molecules are also used to induce the differentiation of neural stem cells and pluripotent stem cells (Amaral et al., 2019; Olivier et al., 2016). In this study, we found that SAG, a small molecular agonist of Shh signaling, could promote the NP-specific differentiation of ADSCs.

The gene and protein expression levels of aggrecan, SOX9, and collagen II were used to assess the ECM synthesis of cells. Both NP cells and chondrocytes have high expression of aggrecan, SOX9, and COL2, so we chose KRT19, PAX1, and Cd24 to indicate the NP-specific differentiation of ADSCs, while Gdf10 was used as a specific marker of chondrogenic differentiation (Minogue et al., 2010; Pattappa et al., 2012; Rutges et al., 2010). Fourteen days after induction with SAG, ADSCs differentiated into an NP-specific phenotype with high expression levels of KRT19 and Cd24 and low expression level of GDF10. SAG also increased the expression levels of aggrecan, SOX9, and collagen II and promoted the synthesis of GAG in ADSCs. In addition, SAG at a concentration of 0.5

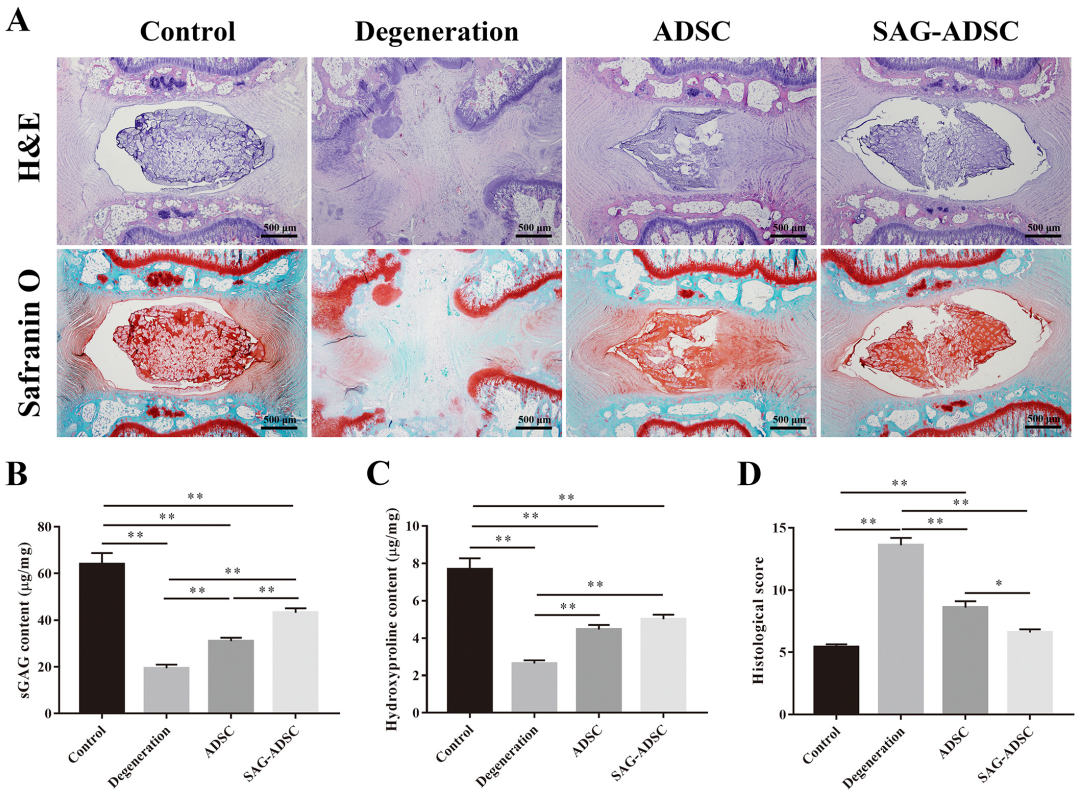

Fig. 6. SAG-treated ADSCs promoted the regeneration of degenerated IVD. (A) Representative H&E and Safranine O staining of discs from different groups were observed. All samples were harvested at 16 weeks after injection. Scale bars = 500 μm. (B) The content of sGAG in each group at 16 weeks after injection were quantified by Blyscan assay. (C) The content of hydroxyproline in each group at 16 weeks after injection was detected by Hydroxyproline Assay Kit. (D) Histological grade of each group was evaluated at 16 weeks after injection. Data represent mean ± SEM. $*P < 0.05$, $**P < 0.01$.

μM is efficient enough to induce an NP-specific differentiation of ADSCs. We have already demonstrated that TGF-β3 has the ability to induce an NP-like differentiation of MSCs (Tao et al., 2015). Other research groups have also reported similar conclusions in previous studies (Gan et al., 2016; Zhu et al., 2017). However, TGF-β3 is also used to induce a chondrogenic differentiation of stem cells (Huang et al., 2018; Qu et al., 2019). Therefore, the NP-like differentiation induced by TGF-β3 is not specific and needs to be improved. In the current study, TGF-β3 was added to the differentiation medium. After SAG was added to the differentiation medium, the efficiency of the NP-specific differentiation of ADSCs was significantly increased. These results indicated that the SAG and TGF-β3 synergy was better than TGF-β3 alone for inducing ADSC differentiation towards an NP cell phenotype.

Both TGF-β and Shh signaling pathways were activated during the NP-specific differentiation of ADSCs. When the TGF-β signaling pathway was activated, the Shh signaling pathway was activated without SAG induction. In addition, when activation of the TGF-β signaling pathway was inhibited, the Shh signaling pathway activated by SAG could also be partly blocked. However, the activation of the Shh signaling pathway cannot affect the TGF-β signaling pathway. The TGF-β signaling pathway is important in the NP-like differentiation and chondrogenic differentiation of MSCs (Colombier et al., 2016; Hara et al., 2016; Zhou et al., 2015). The Shh signaling pathway also plays an important role in the NP-specific differentiation of MSCs (Choi and Harfe, 2011; Dahia et al., 2009). In our study, the activation of the Shh signaling pathway seemed to be dependent on TGF-β signaling. In fact, the TGF-β and Shh signaling pathways play roles mainly in different stages of differentiation. In the early stage of NP-specific differentiation, the TGF-β signaling pathway increases the expression levels of related molecules in the Shh signaling pathway and promotes the differentiation of stem cells (Li et al., 2013). In the later stage of differentiation, the Shh signaling pathway is activated consistently and leads to NP-specific differentiation (Choi et al., 2008). Kopesky et al. (2011) reported that the simple activation of the TGF-β signaling pathway is more likely to induce MSC differentiation towards a chondrogenic phenotype. The use of SAG promoted the activation of the Shh signaling pathway and increased the efficiency of NP-specific differentiation.

Rat tail disc degeneration models have been used in many disc regeneration research studies (Ching et al., 2004; Lotz and Chin, 2000). A needle puncture rat-tail degeneration model is widely used because of its greatly simplified procedure without major surgery (Cunha et al., 2017; Han et al., 2008). The microenvironment in the degenerated NP is suboptimal and negatively influences the survival and function of

transplanted cells (Huang et al., 2013; Kregar Velikonja et al., 2014). Our *in vivo* study showed that ADSCs pretreated with SAG significantly increased GAG and collagen II synthesis and recovered the NP structure. We believe this is because the NP-specific differentiated ADSCs are more able to tolerate the harsh microenvironment in the degenerated NP than the undifferentiated ADSCs (Okuma et al., 2000). However, significant differences could still be observed between the control and SAG-ADSCs groups, which indicated that ADSCs pretreated with SAG can only partly regenerate the degenerated NP. More research should be carried out to improve the induction efficiency of NP-specific differentiation and the NP regenerative ability in ADSCs.

In this study, we demonstrated that SAG at a concentration of 0.5 μM can activate the Shh signaling pathway and increase the ECM synthesis and NP-specific differentiation of ADSCs. Simply activating the TGF-β signaling pathway has a low efficiency in inducing NP-specific differentiation of ADSCs. Both TGF-β and Shh signaling pathways are needed during the NP-specific differentiation of ADSCs, and activation of the TGF-β signaling pathway can promote the activation of Shh signaling. SAG pretreated ADSCs can also promote the regeneration of degenerated IVDs *in vivo*.

Disclosure

The authors have no potential conflicts of interest to disclose.

ACKNOWLEDGMENTS

This study was partly supported by grants from the National Nature Science Foundation of China (81572177 and 81772379), and the General Science and Technology Planning Project (2016C33151) and Nature Science Foundation (LQ18H060003) of Zhejiang Province, and China Postdoctoral Science Foundation (2017M612011).

ORCID

Jianming Hua https://orcid.org/0000-0003-1902-8874
Ning Shen https://orcid.org/0000-0001-8686-5459
Jingkai Wang https://orcid.org/0000-0003-4905-3595
Yiqing Tao https://orcid.org/0000-0002-4390-3758
Fangcai Li https://orcid.org/0000-0002-2402-781X
Qixin Chen https://orcid.org/0000-0002-1768-8732
Xiaopeng Zhou https://orcid.org/0000-0002-0650-183X

REFERENCES

Amaral, J.D., Silva, D., Rodrigues, C.M.P., Sola, S., and Santos, M.M.M. (2019). A novel small molecule p53 stabilizer for brain cell differentiation. Front. Chem. *7*, 15.

Amirpour, N., Amirizade, S., Hashemibeni, B., Kazemi, M., Hadian, M., and Salehi, H. (2019). Differentiation of eye field neuroectoderm from human adipose-derived stem cells by using small-molecules and hADSC-conditioned medium. Ann. Anat. *221*, 17-26.

Andersson, G.B. (1999). Epidemiological features of chronic low-back pain. Lancet *354*, 581-585.

Briscoe, J. and Small, S. (2015). Morphogen rules: design principles of gradient-mediated embryo patterning. Development *142*, 3996-4009.

Chen, J., Yan, W., and Setton, L.A. (2006). Molecular phenotypes of notochordal cells purified from immature nucleus pulposus. Eur. Spine J. *15* Suppl 3, S303-S311.

Chen, J.K., Taipale, J., Young, K.E., Maiti, T., and Beachy, P.A. (2002). Small molecule modulation of Smoothened activity. Proc. Natl. Acad. Sci. U. S. A. *99*, 14071-14076.

Chen, L., Liu, G., Li, W., and Wu, X. (2019). Chondrogenic differentiation of bone marrow-derived mesenchymal stem cells following transfection with Indian hedgehog and sonic hedgehog using a rotary cell culture system. Cell. Mol. Biol. Lett. *24*, 16.

Ching, C.T., Chow, D.H., Yao, F.Y., and Holmes, A.D. (2004). Changes in nuclear composition following cyclic compression of the intervertebral disc in an in vivo rat-tail model. Med. Eng. Phys. *26*, 587-594.

Choi, K.S., Cohn, M.J., and Harfe, B.D. (2008). Identification of nucleus pulposus precursor cells and notochordal remnants in the mouse: implications for disk degeneration and chordoma formation. Dev. Dyn. *237*, 3953-3958.

Choi, K.S. and Harfe, B.D. (2011). Hedgehog signaling is required for formation of the notochord sheath and patterning of nuclei pulposi within the intervertebral discs. Proc. Natl. Acad. Sci. U. S. A. *108*, 9484-9489.

Choi, K.S., Lee, C., and Harfe, B.D. (2012). Sonic hedgehog in the notochord is sufficient for patterning of the intervertebral discs. Mech. Dev. *129*, 255-262.

Colombier, P., Clouet, J., Boyer, C., Ruel, M., Bonin, G., Lesoeur, J., Moreau, A., Fellah, B.H., Weiss, P., Lescaudron, L., et al. (2016). TGF-beta1 and GDF5 act synergistically to drive the differentiation of human adipose stromal cells toward nucleus pulposus-like cells. Stem Cells *34*, 653-667.

Cunha, C., Almeida, C.R., Almeida, M.I., Silva, A.M., Molinos, M., Lamas, S., Pereira, C.L., Teixeira, G.Q., Monteiro, A.T., Santos, S.G., et al. (2017). Systemic delivery of bone marrow mesenchymal stem cells for in situ intervertebral disc regeneration. Stem Cells Transl. Med. *6*, 1029-1039.

Dahia, C.L., Mahoney, E., and Wylie, C. (2012). Shh signaling from the nucleus pulposus is required for the postnatal growth and differentiation of the mouse intervertebral disc. PLoS One *7*, e35944.

Dahia, C.L., Mahoney, E.J., Durrani, A.A., and Wylie, C. (2009). Intercellular signaling pathways active during intervertebral disc growth, differentiation, and aging. Spine (Phila Pa 1976) *34*, 456-462.

Eyring, E.J. (1969). The biochemistry and physiology of the intervertebral disk. Clin. Orthop. Relat. Res. *67*, 16-28.

Fontana, G., Thomas, D., Collin, E., and Pandit, A. (2014). Microgel microenvironment primes adipose-derived stem cells towards an NP cells-like phenotype. Adv. Healthc. Mater. *3*, 2012-2022.

Gan, Y., Li, S., Li, P., Xu, Y., Wang, L., Zhao, C., Ouyang, B., Tu, B., Zhang, C., Luo, L., et al. (2016). A controlled release codelivery system of MSCs encapsulated in dextran/gelatin hydrogel with TGF-beta3-loaded nanoparticles for nucleus pulposus regeneration. Stem Cells Int. *2016*, 9042019.

Han, B., Zhu, K., Li, F.C., Xiao, Y.X., Feng, J., Shi, Z.L., Lin, M., Wang, J., and Chen, Q.X. (2008). A simple disc degeneration model induced by percutaneous needle puncture in the rat tail. Spine (Phila Pa 1976) *33*, 1925-1934.

Hara, E.S., Ono, M., Yoshioka, Y., Ueda, J., Hazehara, Y., Pham, H.T., Matsumoto, T., and Kuboki, T. (2016). Antagonistic effects of insulin and TGF-beta3 during chondrogenic differentiation of human BMSCs under a minimal amount of factors. Cells Tissues Organs *201*, 88-96.

Huang, L., Yi, L., Zhang, C., He, Y., Zhou, L., Liu, Y., Qian, L., Hou, S., and Weng, T. (2018). Synergistic effects of FGF-18 and TGF-beta3 on the chondrogenesis of human adipose-derived mesenchymal stem cells in the pellet culture. Stem Cells Int. *2018*, 7139485.

Huang, Y.C., Leung, V.Y., Lu, W.W., and Luk, K.D. (2013). The effects of microenvironment in mesenchymal stem cell-based regeneration of intervertebral disc. Spine J. *13*, 352-362.

Jia, J., Wang, S.Z., Ma, L.Y., Yu, J.B., Guo, Y.D., and Wang, C. (2018). The differential effects of leukocyte-containing and pure platelet-rich plasma

on nucleus pulposus-derived mesenchymal stem cells: implications for the clinical treatment of intervertebral disc degeneration. Stem Cells Int. *2018*, 7162084.

Jing, H., Zhang, X., Gao, M., Luo, K., Fu, W., Yin, M., Wang, W., Zhu, Z., Zheng, J., and He, X. (2019). Kartogenin preconditioning commits mesenchymal stem cells to a precartilaginous stage with enhanced chondrogenic potential by modulating JNK and beta-catenin-related pathways. FASEB J. *33*, 5641-5653.

Komada, M. (2012). Sonic hedgehog signaling coordinates the proliferation and differentiation of neural stem/progenitor cells by regulating cell cycle kinetics during development of the neocortex. Congenit. Anom. (Kyoto) *52*, 72-77.

Kopesky, P.W., Vanderploeg, E.J., Kisiday, J.D., Frisbie, D.D., Sandy, J.D., and Grodzinsky, A.J. (2011). Controlled delivery of transforming growth factor beta1 by self-assembling peptide hydrogels induces chondrogenesis of bone marrow stromal cells and modulates Smad2/3 signaling. Tissue Eng. Part A *17*, 83-92.

Kregar Velikonja, N., Urban, J., Frohlich, M., Neidlinger-Wilke, C., Kletsas, D., Potocar, U., Turner, S., and Roberts, S. (2014). Cell sources for nucleus pulposus regeneration. Eur. Spine J. *23* Suppl 3, S364-S374.

Lee, C.R., Sakai, D., Nakai, T., Toyama, K., Mochida, J., Alini, M., and Grad, S. (2007). A phenotypic comparison of intervertebral disc and articular cartilage cells in the rat. Eur. Spine J. *16*, 2174-2185.

Lewis, C. and Krieg, P.A. (2014). Reagents for developmental regulation of Hedgehog signaling. Methods *66*, 390-397.

Li, T., Longobardi, L., Myers, T.J., Temple, J.D., Chandler, R.L., Ozkan, H., Contaldo, C., and Spagnoli, A. (2013). Joint TGF-beta type II receptor-expressing cells: ontogeny and characterization as joint progenitors. Stem Cells Dev. *22*, 1342-1359.

Lotz, J.C. and Chin, J.R. (2000). Intervertebral disc cell death is dependent on the magnitude and duration of spinal loading. Spine (Phila Pa 1976) *25*, 1477-1483.

Minogue, B.M., Richardson, S.M., Zeef, L.A., Freemont, A.J., and Hoyland, J.A. (2010). Characterization of the human nucleus pulposus cell phenotype and evaluation of novel marker gene expression to define adult stem cell differentiation. Arthritis Rheum. *62*, 3695-3705.

Okuma, M., Mochida, J., Nishimura, K., Sakabe, K., and Seiki, K. (2000). Reinsertion of stimulated nucleus pulposus cells retards intervertebral disc degeneration: an in vitro and in vivo experimental study. J. Orthop. Res. *18*, 988-997.

Olivier, E.N., Marenah, L., McCahill, A., Condie, A., Cowan, S., and Mountford, J.C. (2016). High-efficiency serum-free feeder-free erythroid differentiation of human pluripotent stem cells using small molecules. Stem Cells Transl. Med. *5*, 1394-1405.

Pattappa, G., Li, Z., Peroglio, M., Wismer, N., Alini, M., and Grad, S. (2012). Diversity of intervertebral disc cells: phenotype and function. J. Anat. *221*, 480-496.

Qu, D., Zhu, J.P., Childs, H.R., and Lu, H.H. (2019). Nanofiber-based transforming growth factor-beta3 release induces fibrochondrogenic differentiation of stem cells. Acta Biomater. *93*, 111-122.

Richardson, S.M., Kalamegam, G., Pushparaj, P.N., Matta, C., Memic, A., Khademhosseini, A., Mobasheri, R., Poletti, F.L., Hoyland, J.A., and Mobasheri, A. (2016). Mesenchymal stem cells in regenerative medicine: focus on articular cartilage and intervertebral disc regeneration. Methods *99*, 69-80.

Rutges, J., Creemers, L.B., Dhert, W., Milz, S., Sakai, D., Mochida, J., Alini, M., and Grad, S. (2010). Variations in gene and protein expression in human nucleus pulposus in comparison with annulus fibrosus and cartilage cells: potential associations with aging and degeneration. Osteoarthritis Cartilage *18*, 416-423.

Sakai, D. and Andersson, G.B. (2015). Stem cell therapy for intervertebral disc regeneration: obstacles and solutions. Nat. Rev. Rheumatol. *11*, 243-256.

Seifert, K., Buttner, A., Rigol, S., Eilert, N., Wandel, E., and Giannis, A. (2012). Potent small molecule Hedgehog agonists induce VEGF expression in vitro. Bioorg. Med. Chem. *20*, 6465-6481.

Stanton, B.Z. and Peng, L.F. (2010). Small-molecule modulators of the Sonic Hedgehog signaling pathway. Mol. Biosyst. *6*, 44-54.

Tam, V., Rogers, I., Chan, D., Leung, V.Y., and Cheung, K.M. (2014). A comparison of intravenous and intradiscal delivery of multipotential stem cells on the healing of injured intervertebral disk. J. Orthop. Res. *32*, 819-825.

Tao, Y., Zhou, X., Liang, C., Li, H., Han, B., Li, F., and Chen, Q. (2015). TGF-beta3 and IGF-1 synergy ameliorates nucleus pulposus mesenchymal stem cell differentiation towards the nucleus pulposus cell type through MAPK/ERK signaling. Growth Factors *33*, 326-336.

Tsaryk, R., Gloria, A., Russo, T., Anspach, L., De Santis, R., Ghanaati, S., Unger, R.E., Ambrosio, L., and Kirkpatrick, C.J. (2015). Collagen-low molecular weight hyaluronic acid semi-interpenetrating network loaded with gelatin microspheres for cell and growth factor delivery for nucleus pulposus regeneration. Acta Biomater. *20*, 10-21.

Vaudreuil, N., Henrikson, K., Pohl, P., Lee, A., Lin, H., Olsen, A., Dong, Q., Dombrowski, M., Kang, J., Vo, N., et al. (2018). Photopolymerizable biogel scaffold seeded with mesenchymal stem cells: safety and efficacy evaluation of novel treatment for intervertebral disc degeneration. J. Orthop. Res. *37*, 1451-1459.

Vazin, T., Ashton, R.S., Conway, A., Rode, N.A., Lee, S.M., Bravo, V., Healy, K.E., Kane, R.S., and Schaffer, D.V. (2014). The effect of multivalent Sonic hedgehog on differentiation of human embryonic stem cells into dopaminergic and GABAergic neurons. Biomaterials *35*, 941-948.

Vos, T., Flaxman, A.D., Naghavi, M., Lozano, R., Michaud, C., Ezzati, M., Shibuya, K., Salomon, J.A., Abdalla, S., Aboyans, V., et al. (2012). Years lived with disability (YLDs) for 1160 sequelae of 289 diseases and injuries 1990-2010: a systematic analysis for the Global Burden of Disease Study 2010. Lancet *380*, 2163-2196.

Wang, S.Z., Rui, Y.F., Lu, J., and Wang, C. (2014). Cell and molecular biology of intervertebral disc degeneration: current understanding and implications for potential therapeutic strategies. Cell Prolif. *47*, 381-390.

Wang, Y., Han, C., Lu, L., Magliato, S., and Wu, T. (2013). Hedgehog signaling pathway regulates autophagy in human hepatocellular carcinoma cells. Hepatology *58*, 995-1010.

Yang, W., Zheng, Y., Chen, J., Zhu, Q., Feng, L., Lan, Y., Zhu, P., Tang, S., and Guo, R. (2019). Preparation and characterization of the collagen/cellulose nanocrystals/USPIO scaffolds loaded kartogenin for cartilage regeneration. Mater. Sci. Eng. C Mater. Biol. Appl. *99*, 1362-1373.

Yao, P.J., Petralia, R.S., and Mattson, M.P. (2016). Sonic hedgehog signaling and hippocampal neuroplasticity. Trends Neurosci. *39*, 840-850.

Zhou, X., Tao, Y., Chen, E., Wang, J., Fang, W., Zhao, T., Liang, C., Li, F., and Chen, Q. (2018a). Genipin-cross-linked type II collagen scaffold promotes the differentiation of adipose-derived stem cells into nucleus pulposus-like cells. J. Biomed. Mater. Res. A *106*, 1258-1268.

Zhou, X., Tao, Y., Wang, J., Liang, C., Wang, J., Li, H., and Chen, Q. (2015). Roles of FGF-2 and TGF-beta/FGF-2 on differentiation of human mesenchymal stem cells towards nucleus pulposus-like phenotype. Growth Factors *33*, 23-30.

Zhou, X., Wang, J., Fang, W., Tao, Y., Zhao, T., Xia, K., Liang, C., Hua, J., Li, F., and Chen, Q. (2018b). Genipin cross-linked type II collagen/chondroitin sulfate composite hydrogel-like cell delivery system induces differentiation of adipose-derived stem cells and regenerates degenerated nucleus pulposus. Acta Biomater. *71*, 496-509.

Zhu, Y., Tan, J., Zhu, H., Lin, G., Yin, F., Wang, L., Song, K., Wang, Y., Zhou, G., and Yi, W. (2017). Development of kartogenin-conjugated chitosan-hyaluronic acid hydrogel for nucleus pulposus regeneration. Biomater. Sci. *5*, 784-791.